Hindawi
Advances in Meteorology
Volume 2018, Article ID 5712046, 17 pages
https://doi.org/10.1155/2018/5712046

Research Article

Spatiotemporal Variability of Arctic Soil Moisture Detected from High-Resolution RADARSAT-2 SAR Data

Adam Collingwood,[1,2] François Charbonneau,[3] Chen Shang,[1] and Paul Treitz[1]

[1]*Department of Geography and Planning, Queen's University, Kingston, ON, Canada K7L 3N6*
[2]*Waterton Lakes National Park, Parks Canada, Box 200, Waterton Park, AB, Canada T0K 2M0*
[3]*Canada Centre for Mapping and Earth Observation, Natural Resources Canada, 560 Rochester Street, Ottawa, ON, Canada K1A 0E4*

Correspondence should be addressed to Paul Treitz; paul.treitz@queensu.ca

Received 17 February 2018; Revised 10 April 2018; Accepted 9 May 2018; Published 26 June 2018

Academic Editor: Jifu Yin

Various methods are used to determine soil moisture information from synthetic aperture radar (SAR) data, but none specific to High Arctic regions and their unique physical characteristics. This research presents a method for determining, at high spatial and temporal resolutions, surface soil moisture and its changes through time in the Canadian High Arctic. An artificial neural network (ANN) is implemented using input variables derived from RADARSAT-2 SAR data and previously modelled surface roughness information. The model is applied to SAR data collected at various incidence angles and acquisition dates across two study sites on Melville Island, Nunavut. The model results in absolute soil moisture errors of approximately 15% ($r^2 = 0.46$) for the primary study sites and 12% ($r^2 = 0.26$) for the verification study area. The ANN model is accurate for modelling (i) the spatial distribution of soil moisture and (ii) the changes in moisture through time across the study areas, two characteristics that are very important for inputs to hydrologic or climate models. In addition, the models appear to be scalable when applied at coarser spatial resolutions, showing potential for large-area mapping or modelling.

1. Introduction

The estimation or modelling of biogeophysical variables such as soil moisture in the Arctic is an important step towards understanding Arctic energy fluxes, the effects of changing climate, and hydrological processes and patterns. For example, the spatial patterns of carbon dioxide (CO_2) fluxes are heavily influenced by the spatial patterns of soil moisture in high-latitude ecosystems [1–7]. Areas in the Arctic with high soil moisture content are also thought to be less responsive to climate warming [3, 5, 8], thus making soil moisture an important variable in global climate-change models. Current and future climate variations in the Arctic will influence the spatial distribution of soil water content, which can affect vegetation, active layer depths, and formation of wetlands over large time scales [9–12]. A more comprehensive understanding of the spatial distribution of soil moisture across the tundra landscape will allow for more accurate and precise predictions of CO_2 flux as ecosystems adapt to climate change [6, 13]. Further, hydrologic variables are very important controls on Arctic geomorphology and ecosystem dynamics [14].

With traditional soil moisture measurement techniques, such as direct sampling (weighing wet soil versus dry soil) and time-domain reflectometry (TDR) measurements, the soil moisture values obtained represent point locations only and are usually averaged or extrapolated over large areas [15]. Spatial variation in soil moisture levels is an important consideration at a number of spatial scales. At subcatchment and finer scales in particular, the spatial distribution of soil moisture becomes as (or more) important than the absolute value of the soil moisture [16]. The demand for spatially distributed soil moisture is clear, but point measurement data are often insufficient, that is, due to soil heterogeneity,

land use, and topography. In short, soil moisture may be very different in space and time from one point to another [17–19].

Information gathered from synthetic aperture radar (SAR) is ideal for the spatial estimation or modelling of soil moisture, at a range of different spatial scales [20–22]. In many cases, these data can be gathered instantaneously over large areas, day or night, in any weather, which is a tremendous advantage over traditional techniques. SAR data are especially useful for medium- and large-scale analysis of soil moisture levels [16, 23, 24]. However, there has been limited research on SAR-modelled soil moisture conducted in the Arctic [25–28], or in natural (nonagricultural) environments in general. Jagdhuber et al. [29] examined the utility of multitemporal space-borne C-band SAR polarimetry for estimating soil freezing and thawing states and found that the mean scattering alpha angle and polarimetric entropy were strongly correlated with the soil freezing and thawing states. A more recent study by Högström and Bartsch [28] identified the fraction of water bodies as a source of error in coarse-scale SAR-retrieved soil moisture due to variations in water surface roughness. However, high-resolution multi-incidence angle SAR data from sensors such as RADARSAT-2 have not been examined to any significant degree for their utility in modelling surface moisture conditions in the High Arctic at fine spatial scales.

There are a number of methods for deriving soil moisture values from SAR backscatter, each possessing certain advantages and disadvantages. Regression-based empirical models, such as those of Dubois et al. [20], are often used to model soil moisture [30–33]. However, empirical models require large quantities of field data and are often very site specific [34]. Physical models, the most common of which is the integrated equation model (IEM) [35], invert backscatter from inputs including radar parameters, surface roughness, and vegetation cover to derive soil moisture values [34–40]. Physical models, like empirical models, are difficult to apply over large areas, and detailed information on parameters such as topography and soil type is required. Artificial neural networks (ANNs) are commonly used to model surface parameters from SAR data [18, 41] and show great promise in both simplifying the modelling process and increasing the accuracy of the results. ANNs have the capacity to "learn" complex, nonlinear patterns and generalize these patterns in noisy environments [42, 43]. This capacity to generalize means that ANNs can be effective in situations where data may be missing or imprecise. ANNs are also able to incorporate prior knowledge and physical constraints into the analysis, while making no assumptions about the statistical nature of the input data [44, 45]. This allows for the incorporation of disparate data from many remote sensing and ancillary sources, including other ANN model outputs. ANNs are superior to empirical models for generalizing results for application to new areas [46] and do not have the same parameterization problems and assumption requirements as physical models (e.g., IEM).

Given the spatial detail captured by RADARSAT-2 SAR data and the utility of ANNs for modelling environmental variables, we designed a study to model soil moisture in the Canadian High Arctic. The objectives of the research presented here are to (i) examine the relationships that exist between SAR backscatter parameters and surface soil moisture, (ii) model those relationships using an ANN, and (iii) map the spatiotemporal dynamics of Arctic soil moisture using multitemporal RADARSAT-2 imagery acquired with varying incidence angles.

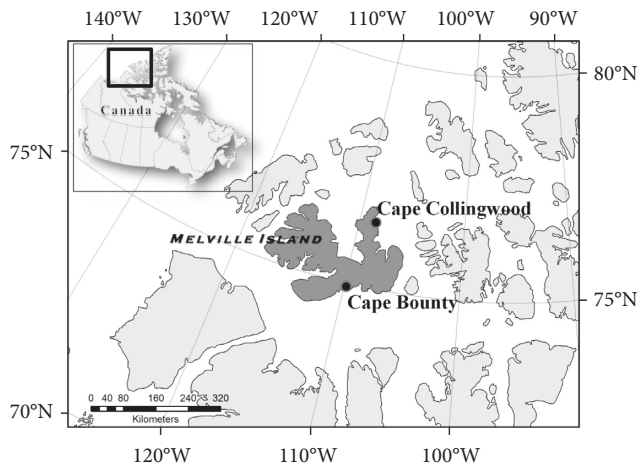

Figure 1: Study area location in the Canadian High Arctic.

2. Methods

2.1. Site Description. The majority of the field work for this study was undertaken at the Cape Bounty Arctic Watershed Observatory (CBAWO), located on the southern coast of Melville Island, Nunavut, Canada (74.91°N, 109.44°W) (Figure 1) in 2009 and 2010. The CBAWO was used to develop, calibrate, and validate the ANN models. This High Arctic site is composed of two parallel watersheds, each covering approximately 15 km^2. The area is characterized by rolling topography of low to medium relief, with elevation varying between 5 m and 125 m above sea level. The site has been impacted by periods of glaciation, during which various tills have been deposited in the study region, including Bolduc, Dundas, and Winter Harbour tills [47]. Winter Harbour till is a thin (1-2 m) carbonate-rich till that contains many mafic and crystalline rock fragments and is draped over the other layers [47]. The Winter Harbour till also offlaps Holocene era fine-grained marine sediments, which are located between approximately 35 m and 90 m above sea level [47, 48]. These sediments are underlain by the Franklinian mobile belt, composed of Paleozoic sandstone, siltstone, and shale [48]. Vegetation in the area is extremely limited and rarely exceeds a few centimetres in height. Greater vegetation biomass is found in sedge and heath communities, while polar desert areas can be completely barren. Large areas of exposed, fractured bedrock are also present, and the entire area is underlain by permafrost, with an active layer of 0.5–1 m during the summer.

Additional field work was conducted in 2011 in the vicinity of Cape Collingwood on the Sabine Peninsula, located on northern Melville Island (approximately 76.53°N,

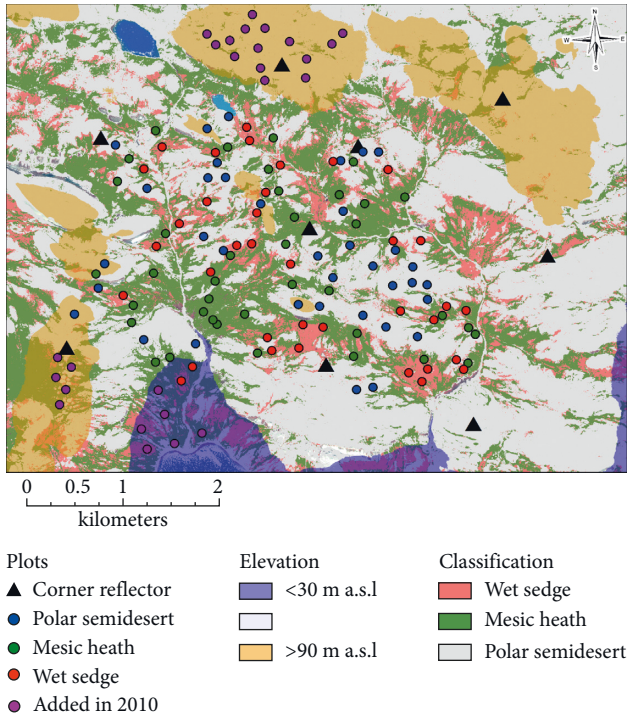

Figure 2: Unsupervised classification, elevation stratification, and plot locations at the Cape Bounty Arctic Watershed Observatory.

108.83°W) (Figure 1). Plots from this more northerly study site are representative of three different underlying bedrock types, all of which are different from the CBAWO. The Kanguk formation consists of a shale bedrock with surface materials of poorly sorted clay-silt mixed with a sand and gravel till; the Hassel formation has a sandstone bedrock with surface materials consisting of sand and silty sand; and the Christopher formation is a shale bedrock with a very fine, poorly drained silty clay surficial material [49]. These different surfaces will test the extension of the models developed at the CBAWO to other areas of the High Arctic. The topography of the area is characterized by low-to-moderate relief, with vegetation similar to the CBAWO and other locations in the High Arctic.

2.2. Field Methods. A digital elevation model (DEM) for the Cape Bounty study area was derived from a high-resolution GeoEye stereopair collected in August 2009. An unsupervised classification was also conducted on the GeoEye imagery, to distinguish between the three main vegetation communities in the region (polar desert, mesic heath, and wet sedge). The DEM and unsupervised classification results were then used to set up a stratified random sampling scheme across three elevations (<30 m, 30–90 m, and >90 m) and three vegetation classes (Figure 2). The number of samples across each vegetation class was determined on a relative basis by the spatial coverage of each class in the unsupervised classification. The elevation groupings were chosen to exploit the current knowledge of different till layers, with marine sediments thought to be present between approximately 35 m and 90 m above sea level, as explained previously. In 2009, 119 sample

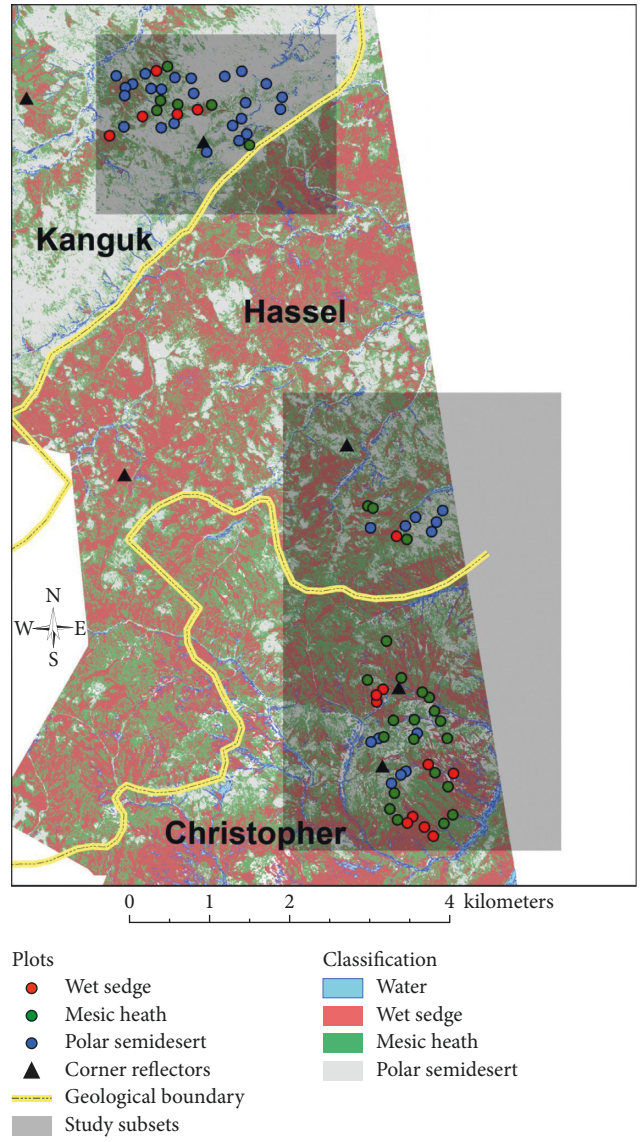

Figure 3: Unsupervised classification, study plots, and geological boundaries for the Cape Bounty Arctic Watershed Observatory.

locations were used, then expanded to 136 locations in 2010 to allow for increased coverage of the elevation classes. This stratified random sampling scheme was designed to obtain soil moisture measurements from areas with as many differences in backscatter-affecting variables as possible. Vegetation, surface roughness, and soil type, in addition to soil moisture, are the main components of a target that affect SAR backscatter response: surface roughness information could not be obtained a priori with the available optical imagery, however, so was not used as a stratification criterion. Similar methods were used at the Cape Collingwood locations, with the DEM and initial unsupervised vegetation classification being generated from a high-resolution 2011 Worldview-2 stereopair. A total of 79 sample plots were used at the Cape Collingwood location (Figure 3).

For both study locations, efforts were made to collect soil moisture measurements at each plot within three hours of the RADARSAT-2 acquisition, in order to minimize any

daily fluctuations in soil moisture. For logistical reasons, this was sometimes expanded to ±6 hours. A meteorological station set up in the CBAWO gave precipitation information, which was used, along with in situ weather observations, to determine the timing and amount of precipitation with regard to overpass times and the temporal stability of the soil moisture measurements.

2.2.1. TDR Methodology. Soil moisture values were taken with a TDR (time-domain reflectometry) instrument, the Moisturepoint MP-917 from Environmental Sensors Inc. A TDR measures the apparent dielectric constant (K_a) of the soil by sending an electromagnetic pulse along a transmission line (i.e., metal probe) in a soil medium, and measuring the propagation velocity. The propagation velocity is influenced by the dielectric constant—higher dielectric values result in a slower velocity, when compared to the transmission velocity in a vacuum:

$$K_a = \left(\frac{c}{v}\right)^2, \tag{1}$$

where c is the speed of light and v is the propagation velocity.

The propagation velocity is determined by measuring the time it takes for a pulse to travel the distance to the end of the transmission line and back. Velocity can therefore be expressed as

$$v = \frac{2L}{t}, \tag{2}$$

where L is the linear distance travelled (probe length) and t is the measured travel time.

The values from the TDR were recorded as travel time, and so can be converted into the dielectric constant K_a by substituting (2) in (1):

$$K_a = \left(\frac{c}{(2L/t)}\right)^2, \tag{3}$$

where c is the speed of light (m/s), L is the length of the probe (mm), and t is the time delay (ns) measured with the TDR probe.

No site-specific calibration of the TDR readings was possible, so universal equations were applied. While not quite as accurate as a site-specific empirical regression could be, universal equations are very close in terms of overall accuracy and are an improvement over factory calibration settings [50]. The apparent dielectric constant was converted to % volumetric soil moisture (θ_v) using a 5°C three-phase model (4), that is, a linear approximation of the Topp universal equation [51, 52] for mineral soil and the Nagare equation [53] for organic soil (5).

$$\theta_v = 0.1209 * \sqrt{K_a} - 0.2032, \tag{4}$$

$$\theta_v = -0.0189 + (0.032 * K_a) - \left(0.000459 * \left(K_a^2\right)\right) + \left(0.0000027 * \left(K_a^3\right)\right). \tag{5}$$

While the Topp equation and its linear approximations have been shown to be accurate for a wide range of mineral soils [50–52], it is suggested very small bulk density values (such as in organic soils) can lead to large errors [54, 55], necessitating a separate equation (5) for low bulk density soils.

Soil moisture values were taken with custom 5 cm length probes, making the moisture values an integrated average of the top 5 cm of the soil. Three measurements per plot were taken in a triangular pattern around the plot center, approximately 2 m apart, with some measurements being taken in the vegetated areas, if present. This is important, as the vegetated areas hold different amounts of water than the mineral soil due to the different properties and bulk density of the heavily organic soils, and different equations are used to transform the TDR values to soil moisture values ((4) and (5)). The value for the plot is a weighted average of the organic and mineral soil moisture values based on an estimate of percent vegetation cover (organic soil) of the plot.

2.3. ANNs. The utility of ANNs in remote sensing (see review in [45]) and as a relatively simple way to invert radar backscatter to surface parameters is well documented [41, 56]. Surface parameter inversion from SAR backscatter data is usually carried out by some sort of linear or nonlinear regression approach [17] or through complex empirical inversion models such as IEM and others [57, 58]. ANNs, however, show great promise in both simplifying this procedure and increasing the accuracy of the results. For example, ANNs were compared to other models [41], that is, the Oh model [59] and the modified Dubois model (MDM) [60]. The ANN models outperformed the Oh model and MDM for surface roughness and soil moisture estimation. The selection of input predictor variables plays a critical role in the performance of ANNs, which may require different variable selection approaches typically adopted for parametric methods (i.e., due to the nonparametric nature of ANN) [61]. From a model specification perspective, the design of an ANN model is of crucial importance to the neural network learning the relationship between the input and output variables. More specifically, the optimal design (i.e., the number of hidden layers and the number of neurons in each layer) may vary across different applications, thus requiring prudent tuning on an individual basis.

However, even though ANNs do not operate based on assumptions regarding the statistical distribution of the input variables, the application of ANN is nontrivial due to the appropriate design and implementation needed to ensure its accuracy and robustness [45]. The performance of a trained ANN can be assessed using root mean square error (RMSE) between observed values and the values predicted by the network. Compared to some machine-learning algorithms that are less vulnerable to high variance, such as support vector machine (SVM), the size of the training sample can have a large impact on the performance of ANN [62]. ANNs learn the characteristics of the data from the sample values, not statistical derivatives. Hence, it is thought that very large numbers of training samples are required to optimally train the ANN, though excessive numbers of samples can slow the training process [45]. Various rules

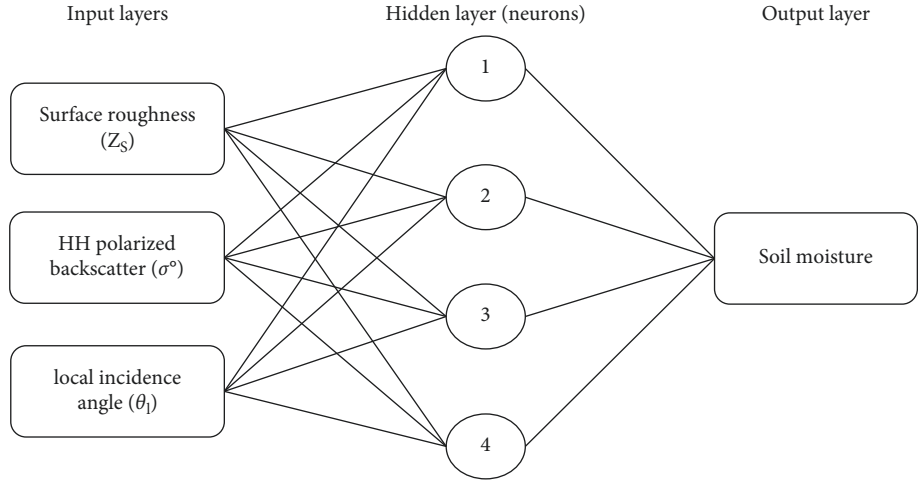

Figure 4: Schematic diagram of the spatially explicit input (and output) layers for the soil moisture ANN model.

have been proposed to determine the optimum number of training samples, for example, 5–10% of the image [63], or $30n(n+1)$ samples [64], with n being the number of input parameters to the ANN. However, these recommendations were for classification applications; that is, no suggestions have been made as to the number of training samples needed for the inversion of a continuous variable, though in this case it would seem that representativeness would be more important than the number of samples. If training samples were not fully representative of soil moisture variability, the predictive accuracy of the ANN model will likely deteriorate, resulting in less comprehensive understanding of the spatial variation of soil moisture over time.

The ANN models for this research were implemented in the MATLAB® software package (MathWorks, Natick, Massachusetts). This implementation is a two-layer (one hidden layer and one output layer) feed-forward network with sigmoid-function hidden neurons and linear-function output neurons, trained with the Levenberg–Marquardt back-propagation algorithm [65] (Figure 4). The input layers included surface roughness (Z_s), HH-polarized backscatter (σ°), and local incidence angle (θ_l). Input data were randomly separated into training (70% of the data), validation (15% of the data), and independent testing data (remaining 15%). Hundreds of models were trained, with each training run having slightly different starting weights and biases for each neuron, as well as randomly selected training data. Different numbers of hidden neurons were also examined, in a trial-and-error approach, until the best model of all the model runs could be selected. The final model for soil moisture had one hidden layer with four neurons (Figure 4).

2.4. Object-Based Image Analysis (OBIA) Methods. The models were built using object-based image analysis (OBIA), which involves pixels being grouped into objects based on the homogeneity of their spatial or spectral characteristics (termed segmentation). OBIA has a number of advantages over pixel-based methods, including reduced dependency on noise-filtering algorithms (especially with SAR data) and the objects being more natural representations of surface properties. OBIA is recognized as a very effective tool for analyzing geospatial and remotely sensed data [66]. With this method, different spatial scales can be investigated by changing the sizes of the image objects. The problem associated with OBIA is finding meaningful scales to investigate, that is, finding the scale of object segmentation that is objectively relevant based on the characteristics of the landscape being studied.

To solve this problem, Drăguţ et al. [67] have developed a tool that integrates with existing OBIA software (eCognition® 8.64) to estimate relevant scale parameters. The tool, ESP (estimation of scale parameter) plots values of local variance (LV) and the rate of change (ROC) of that variance between successive scale levels, that is, against scale levels at a set interval (Figure 5 for an example from the CBAWO). The "scale" of the object is a parameter in the eCognition software that determines the maximum allowed heterogeneity of the image objects, based on user-defined weightings of "color" (pixel values for various image bands) and "shape" (level of object compactness) [68]. In the ESP tool, LV increases with the increase in the scale parameter as the homogeneity of the objects increases; the highest values of LV relative to successive values indicate scales where objects have reached meaningful levels of organization in terms of the variation in their homogeneity. The ROC of the LV is the best way to show this and is a means of identifying how important the respective scale level is in structuring the information on objects' variability relative to the whole scene [67, 69].

The objects were generated from high-resolution optical imagery, 0.5 m pan-sharpened GeoEye-1 imagery for the CBAWO and 0.5 m pan-sharpened Worldview-2 imagery for the Cape Collingwood study site. In both cases, near-infrared, red, and green bands were used for the homogeneity criteria in order for the objects to be physically meaningful, in an ecological sense, on the ground. The Cape Collingwood site was split into two areas, north and south, to aid in processing times. Multiple scales were found to be meaningful (Figure 5), but only the largest (410) and smallest

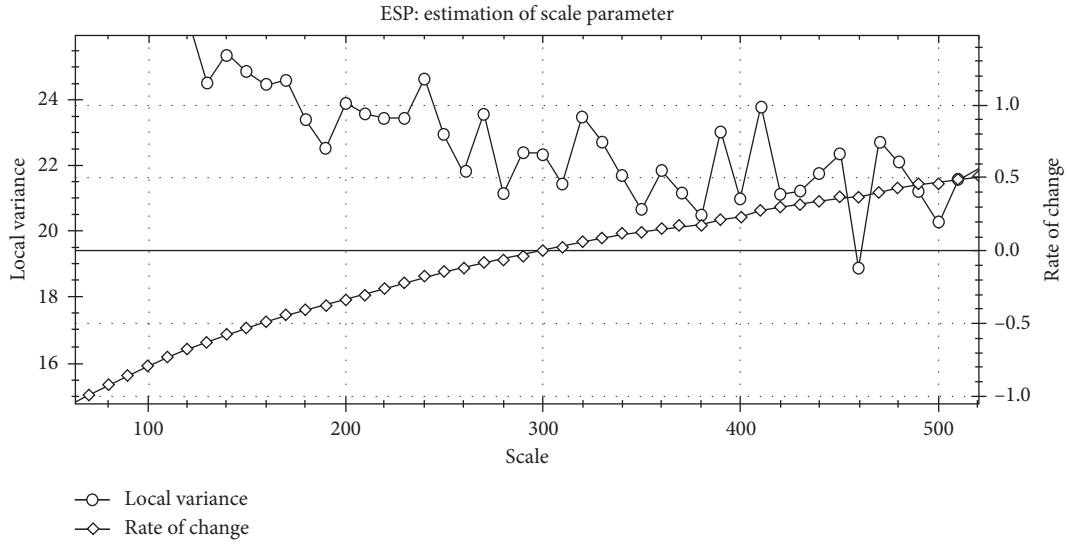

Figure 5: Local variance and rate of change values produced by the ESP tool for the Cape Bounty Arctic Watershed Observatory.

Table 1: RADARSAT-2 data used in the analysis.

RADARSAT-2 beam mode	Avg. incidence angle (°)	Polarization	Spatial resolution (m)	Acquisition date (local time)
U15	41.40	HH	3	01/07/2009
U4	33.00	HH	3	07/07/2010
U26	48.40	HH	3	09/07/2010
U75	25.75	HH	3	11/07/2010
U9	37.00	HH	3	17/07/2010
FQ2[a]	20.90	HH/VV/VH/HV	8	23/07/2010
U21	45.40	HH	3	23/07/2010
U75	25.75	HH	3	04/08/2010
U9	37.00	HH	3	10/08/2010
U8	36.25	HH	3	09/07/2011
U74	24.75	HH	3	10/07/2011
U13	40.00	HH	3	12/07/2011
U79	29.55	HH	3	13/07/2011
U4	33.00	HH	3	23/07/2011

[a]Pass was descending (all others were ascending).

(140) scale parameter values were used in further analysis. The scale values for the small objects at the Cape Collingwood site were slightly different, as the ESP tool estimates the scale parameter based on the local conditions. Scale values of 110 and 160 were used for the small objects for the north and south mapped portions, respectively, and 410 and 400 for the large objects. Small objects for both locations ranged between approximately 50 and 6000 m^2. The larger objects range from about 50 to 35000 m^2. These object sizes could have implications for the SAR spatial resolution requirements for surface roughness and soil moisture modelling.

2.5. SAR Methods. High spatial resolution fully polarimetric (FQ—fine-quad beam mode) and HH-polarized single polarization (U—ultra-fine beam mode) SAR data were collected at various incidence angles over the study areas during the summers of 2009–2011 (Table 1). The calibration of the soil moisture ANN relied on a single date of SAR data to model moisture for that specific date in time. Given that surface soil moisture content can change rapidly through time, only parameters from the date of interest, along with temporally invariant parameters, such as surface roughness, were used to develop the ANN model. The scenes available for different dates were also from different beam modes, with different incidence angles. To examine the capability of the soil moisture ANN model to generalize over other acquisition conditions, it was calibrated with data from one beam mode (one date) and applied to different beam modes from different dates, some with very different average incidence angles. For this reason, the local incidence angle of each image object was also included as a model input variable.

The ultra-fine mode RADARSAT-2 data were orthorectified before further analysis, while the fine-quad data were analyzed in slant range to preserve polarimetric information [70] and were only orthorectified to extract the plot data for each variable after they were calculated for the scene. Nine corner reflectors spaced around the CBAWO, and five around the Cape Collingwood study area, were used to assist with geometric correction. Since an object-based approach

was implemented in the modelling framework, speckle reduction was handled through image averaging at the object level.

2.6. Soil Moisture Models. The relationship between SAR backscatter and soil moisture must be separated from other factors that influence the SAR signal, including surface roughness [71]. Hence, the output of a surface roughness ANN model [72, 73] was included as input to the soil moisture model. More specifically, this surface roughness ANN model was developed using multiangular and polarimetric RADARSAT-2 imagery and field data in an object-based framework for the Cape Bounty and Cape Collingwood study site. To investigate the impact of different spatial scales on surface roughness estimation, analyses were performed on two distinct image object sizes, and consistent performance was observed for both small and large image objects, with normalized RMSEs of approximately 15%. A variety of additional variables were derived and extracted from the SAR data [74], corresponding to the image objects that contained the field-measured soil moisture plots (Table 2). The texture variables were calculated on a per-pixel basis using an 11×11 pixel window for each RADARSAT-2 scene (i.e., HH backscatter intensity), before being averaged for each image object. The texture measures from each scene (and beam mode) were analyzed for correlation individually. Other variables include simple means of the pixel values for each image object.

Variables that were not directly correlated (Pearson $|r| < \sim 0.3$) with the field-measured soil moisture were removed from further analysis. Visual analysis of scatter plots helped to reveal possible nonlinear correlations that the Pearson correlation would not identify. Variables that were highly correlated (Spearman $|\rho| > \sim 0.7$) with other remaining variables were also removed, as multicollinearity can be problematic in the calibration of ANNs [77].

Table 2: Variables generated from SAR data.

Variable	Description
Homogeneity[a]	A measure of local homogeneity
Contrast[a]	A measure of local variation
Correlation[a]	A measure of the linear dependency of grey levels of neighbouring pixels
Mean[a]	Arithmetic mean of all pixel values
SD[a]	Standard deviation of pixel values
VI/VA/VL/U[b]	A normalized log measure of texture
HH	σ^0 intensity of HH polarized backscatter

[a]Haralick et al., [75]. [b]Oliver and Quegan, [76].

3. Results and Discussion

3.1. ANN Model. Of the SAR variables that were examined (Table 2), linear HH backscatter was selected for inclusion in the ANN, as it exhibited stronger correlation to soil moisture than VV and, most importantly, is the only polarization available in both FQ and U beam modes. High temporal coverage was an important consideration for the modelling effort, so variable selection was limited to allow the most possible acquisitions to be used. Reliance on polarimetric parameters, for example, would have (i) excluded the high volume of ultra-fine beam mode data, (ii) limited the model to FQ data, and (iii) reduced the temporal resolution of the analysis. A number of polarimetric variables were examined for completeness, such as Cloude–Pottier decomposition variables [78], intensity ratio, and phase difference, none of which showed strong correlation to soil moisture, something that has been noted in other studies [79].

The variables that were used in the final ANN model were (i) the surface roughness (Z_S) values modelled by the surface roughness ANN [72, 73], (ii) the HH-polarized backscatter (σ°), and (iii) the local incidence angle that corresponds to the HH backscatter used, all averaged across each image object. Of these three variables, the surface roughness is time invariant, so the same values were used across each date for which the model was applied. The σ° values were taken from the scene that corresponds to the date of interest, and the local incidence angle values derived from that same scene. The model was created using the July 11, 2010 U75 CBAWO data, then applied to the other dates for the CBAWO and Cape Collingwood datasets, with the σ° and local incidence angle inputs changing accordingly. A total of 15 plots were not included in the model—five plots had no surface roughness data, and ten were classified as outliers based on the Mahalanobis distances when the inputs were compared to the field-measured moisture. The model was applied to both the small and large image objects at each study location. The results of the ANN modelling are presented in Tables 3–5.

3.2. Cape Bounty Arctic Watershed Observatory. The results for the 2009 and 2010 CBAWO data (Table 3) demonstrate that the best results tend to occur with the steepest incidence angles, that is, the U75 beam mode. Of course, the model was created using the U75 beam mode, but this is also expected due to the nature of the relationship between moisture-affected SAR backscatter and local incidence angles, that is, low incidence angles have been shown to be more accurate for soil moisture prediction [80] since the roughness signal is minimized, leaving moisture as the dominant control on the backscatter. The inclusion of surface roughness and incidence angle information in the ANN allows these differences to be accounted for across different beam modes, but the nature of the relationships between these variables cannot be fully modelled. The modelled soil moisture error is approximately 15% across the various dates and beam modes. Soil moisture values at the CBAWO cover nearly the full range of 0 to 1 m^3/m^3 volumetric water content. When the ANN was applied to the large image objects, the results were similar to the small image objects. The r^2 values are slightly lower, but the RMSE values are comparable.

The ANN soil moisture output, apart from the July 11 U75 data, which were used to create the ANN, is not at the same scale as the field-measured moisture. This difference in scale is because the local incidence angle and σ° backscatter are dependent on the beam mode used. The relationships are still linear, but the slope and intercept of the regression line

Table 3: r^2 and RMSE values of the ANN applied to the different scenes/dates at the CBAWO in 2010.

Date	Beam mode	Avg. inc. angle	Sm. obj. r^2	Sm. obj. RMSE	Lrg. obj. r^2	Lrg. obj. RMSE
1-Jul-2009	U15	43.3	0.15	0.171	—	—
7-Jul-2010	U4	33	0.09	0.210	0.03	0.217
9-Jul-2010	U26	48.4	0.29	0.159	0.18	0.149
11-Jul-2010[a]	U75	25.75	0.75	0.086	0.40	0.118
17-Jul-2010	U9	37	0.39	0.151	0.35	0.121
23-Jul-2010	U21	45.4	0.37	0.173	0.29	0.179
23-Jul-2010[b]	FQ2	20.9	0.31	0.181	—	—
4-Aug-2010	U75	25.75	0.44	0.153	0.32	0.167
10-Aug-2010	U9	37	0.39	0.165	0.32	0.162

Data are presented for both small and large image objects. [a]ANN created using this date. [b]Fine-quad data, descending pass (all others ascending).

Table 4: r^2 and RMSE values of the ANN applied to the different scenes/dates at Cape Collingwood in 2011.

Date	Beam mode	Sm. obj. r^2	Sm. obj. RMSE	Lrg. obj. r^2	Lrg. obj. RMSE
09-Jul-2011[a]	U8	0.13	0.142	0.21	0.136
10-Jul-2011[a]	U74	0.14	0.193	0.27	0.178
12-Jul-2011[b]	U13	0.16	0.163	0.28	0.134
13-Jul-2011[b]	U79	0.20	0.148	0.05	0.135
23-Jul-2011[b]	U4	0.04	0.150	0.05	0.147

[a]Covers northern subset of study area (Kanguk formation). [b]Covers southern subset of study area (Hassel and Christopher formations). Data are presented for both small and large image objects.

Table 5: Results of the ANN applied to the different scenes/dates at Cape Collingwood in 2011, after removal of outlier moss plots.

Date	Beam mode	Sm. obj. r^2	Sm. obj. RMSE	Lrg. obj. r^2	Lrg. obj. RMSE
09-Jul-2011	U8	$0.20^{\uparrow}$	$0.122^{\downarrow}$	$0.32^{\uparrow}$	$0.113^{\downarrow}$
10-Jul-2011	U74	$0.20^{\uparrow}$	$0.172^{\downarrow}$	$0.42^{\uparrow}$	$0.147^{\downarrow}$
12-Jul-2011	U13	$0.19^{\uparrow}$	$0.116^{\downarrow}$	$0.22^{\downarrow}$	$0.119^{\downarrow}$
13-Jul-2011	U79	$0.27^{\downarrow}$	$0.106^{\downarrow}$	$0.03^{\downarrow}$	$0.126^{\downarrow}$
23-Jul-2011	U4	$0.05^{\uparrow}$	$0.151^{\uparrow}$	$0.05^{\leftrightarrow}$	$0.147^{\leftrightarrow}$

Results are presented for both small and large image objects. ↑ = increase from Table 4 values. ↓ = decrease from Table 4 values. ↔ = no change.

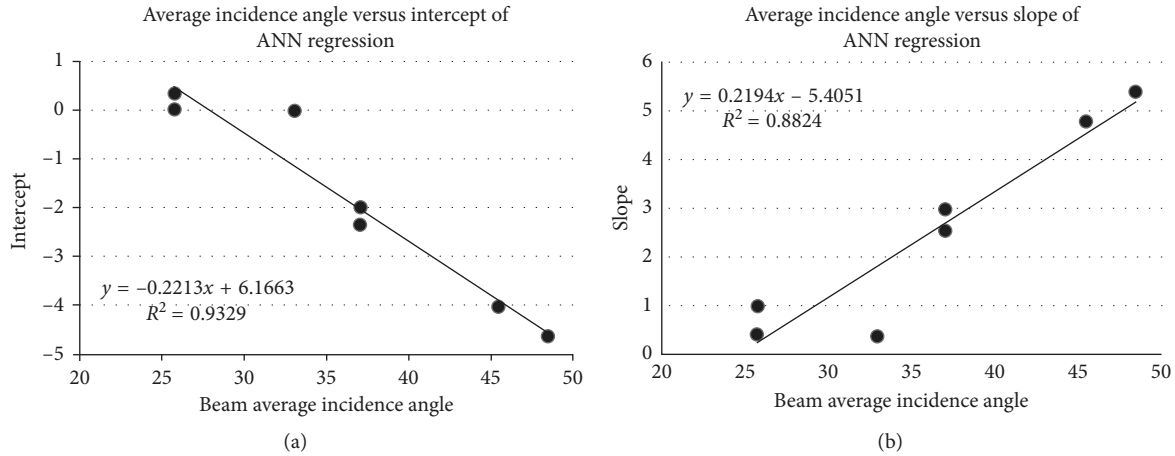

Figure 6: Beam mode incidence angle correlations to slope and intercept values calculated for ANN results.

that relates the ANN output to the field measurements vary by beam mode. However, the differences in the slopes and intercepts correspond closely to the average incidence angle of the beam mode (Figure 6). This relationship can therefore be used to determine the appropriate scaling needed for the ANN output for any given beam mode, even those not available for this study. The r^2 values of the slope and intercept equations are 0.88 and 0.93, respectively, giving high confidence in this relationship between beam average incidence angle and slope/intercept values for the ANN output. The results of the ANN for each different beam mode can be combined once the output scales have been matched

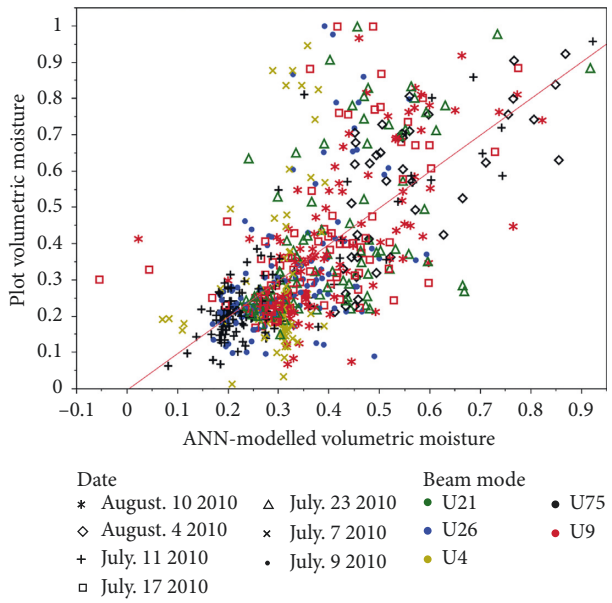

Figure 7: Combined ANN output for each 2010 date, after scaling the results.

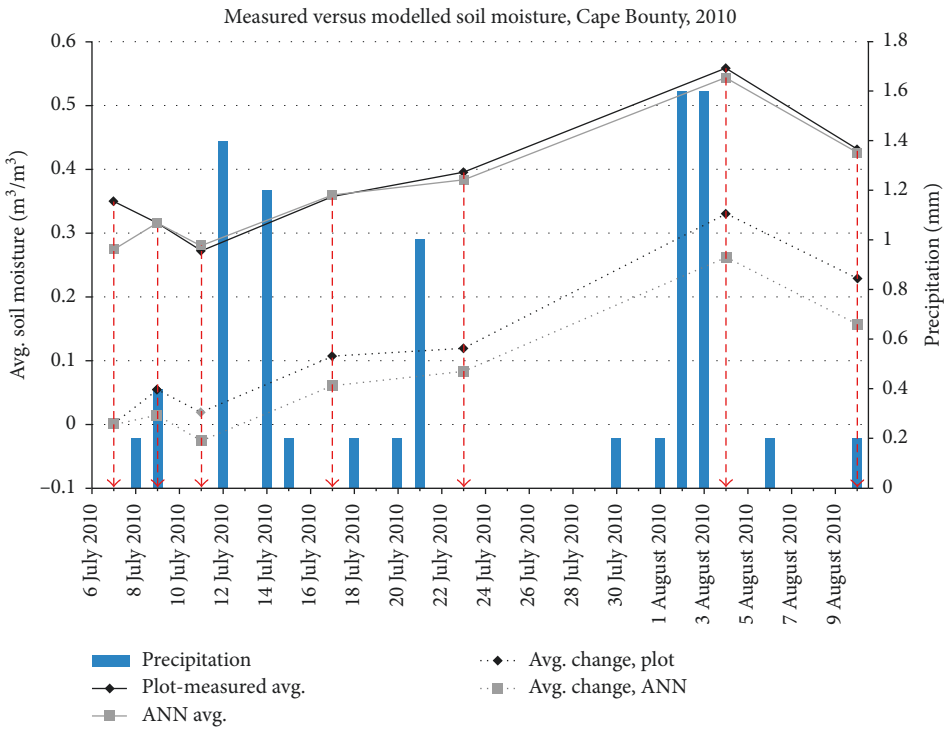

Figure 8: Precipitation and its effects on average soil moisture at the Cape Bounty Arctic Watershed Observatory, 2010. Arrows indicate RADARSAT-2 overpass dates. Plot-measured and ANN avg. values are average soil moisture values measured in the field at each date and the ANN output for that date, respectively. Avg. change values are differences in moisture between each date from a 0 start value (at July 7).

(Figure 7). The r^2 and RMSE values for the combined results are 0.46 and 0.155, respectively.

Once the ANN output is in the same scale as the field-measured soil moisture, then the absolute values can be compared directly. One of the strengths of this methodology is the ability to model soil moisture at different times, and to therefore have a temporal record of soil moisture. The mean soil moisture values across all the plots were compared for each date for which imagery was available and the differences between the field-measured and ANN-modelled moisture values analyzed (Figure 8). The average moisture values given by the ANN model are very similar to the field-measured soil moisture values across all dates (July 7 is the exception). The average soil moisture is affected by the precipitation across the

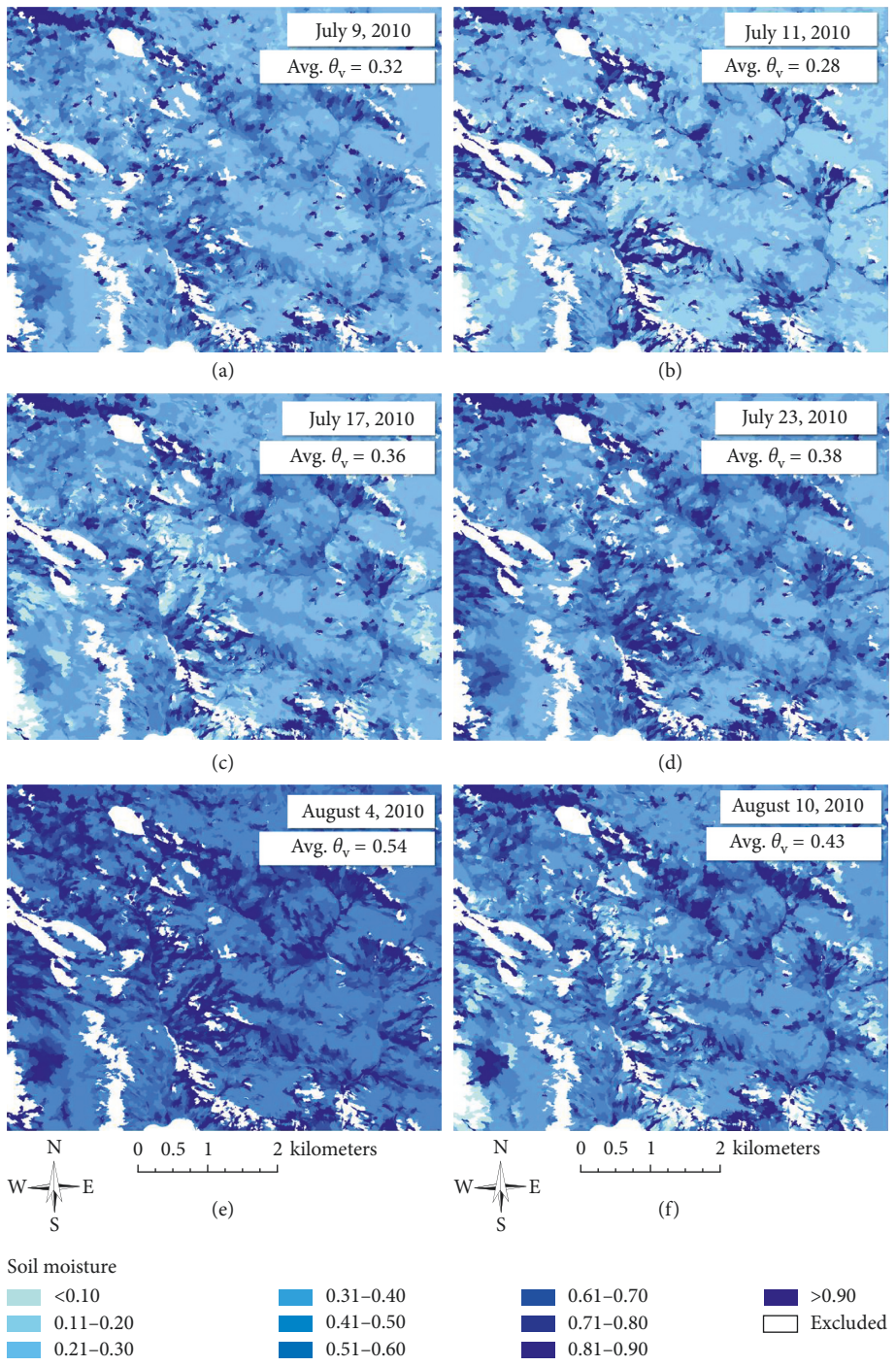

Figure 9: Spatiotemporal distribution of θ_v across 6 dates in 2010 at the Cape Bounty Arctic Watershed Observatory. Average θ_v values are the ANN-modelled averages for the field-measured plots.

area, and this is also reflected in the data. Precipitation data as measured by the CBAWO meteorological station is correlated to increases in average soil moisture, with soil moisture decreasing during periods without precipitation (Figure 8).

The pattern of average soil moisture increases and decreases with weather conditions, a pattern confirmed when the entire study area is modelled for each date. The ANN was applied to every image object for each date, excluding those objects that did not have surface roughness data [72, 73]. Mapping the spatial distribution of soil moisture at such high spatial resolutions is another major strength of the approach taken for this research. The change in moisture across both temporal and spatial scales is readily apparent (Figure 9). Comparing the small to the large image objects reveals the spatial consistency in modelled soil moisture across object sizes (Figure 10).

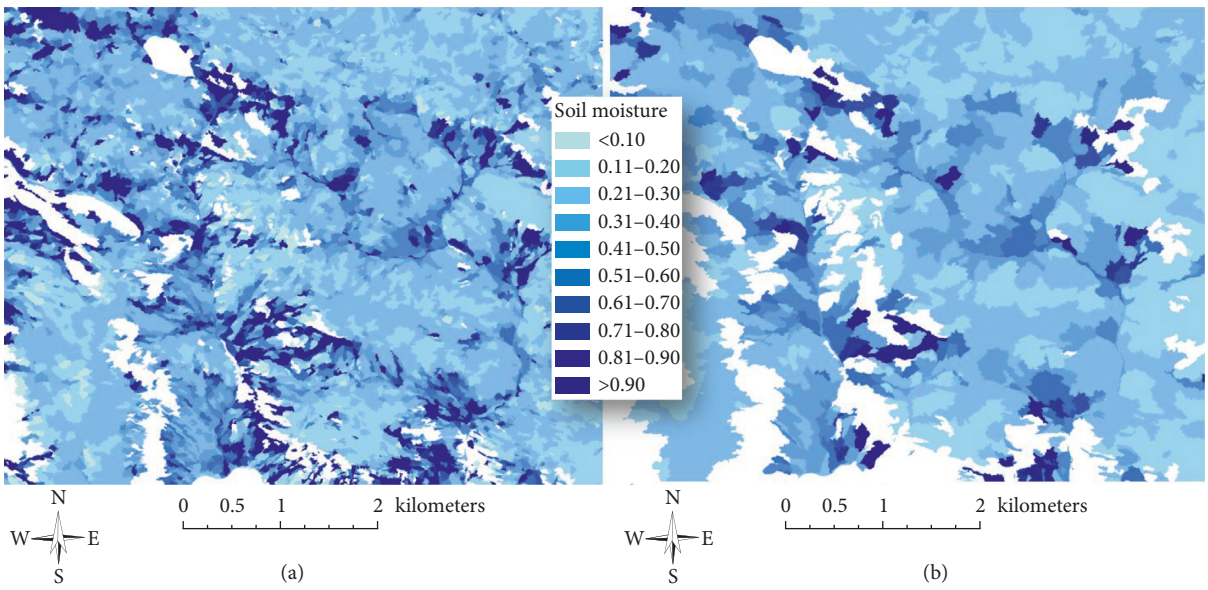

Figure 10: Comparison of ANN-modelled soil moisture for small (a) and large (b) image objects. Values shown are for July 11, 2010.

3.3. Cape Collingwood. In the analysis of the Cape Collingwood data, the July 9 (U8) and the July 10 (U74), 2011 acquisitions cover the northern study area, located in the Kanguk geological formation. The other 2011 acquisitions (Table 2) cover the southern study area, located in the Christopher and Hassel formations.

The results of the ANN model applied to the 2011 imagery are presented in Table 4. The r^2 values are not as strong as for the CBAWO results, though the RMSE values are similar. The total range of moisture values is smaller than at the CBAWO (θ_v of 0.1–0.8 for the northern subset, 0.2–1.0 for the southern subset), giving rise to higher RMSE values on a percentage basis. The July 23 scene resulted in a very poor relationship, although none are particularly strong. It was very wet on July 23, with over 16 mm of rain having fallen over the preceding few days (precipitation measured manually on location with rain gauge) (Figure 8). Unlike the CBAWO ANN results, there is less evidence for incidence angle impacting the accuracy of the results for Cape Collingwood. Beam modes with a small incidence angle, such as U79, have stronger results, while others, such as U74, are no better than the large incidence angle beam mode results (U8, U13).

When the results are scaled to the field-measured soil moisture values and combined (same methodology as for the CBAWO data), the model does not seem to apply as well to Cape Collingwood (Figure 11), though the RMSE values are acceptable. Without the July 23 data included, the combined r^2 and RMSE values are 0.26 and 0.122, respectively. Some of the error in the ANN-modelled moisture values for Cape Collingwood can be attributed to a few plots that are characterized by heavy moss cover, which can have unpredictable effects on SAR backscatter (Figure 12). When these plots are removed (1 plot from North subset, 3 plots from South subset), the results are improved in nearly every case (Table 5).

The absolute values of soil moisture, as has been noted earlier, are not as important as the spatiotemporal results, that is, the modelling of the relative moisture values across

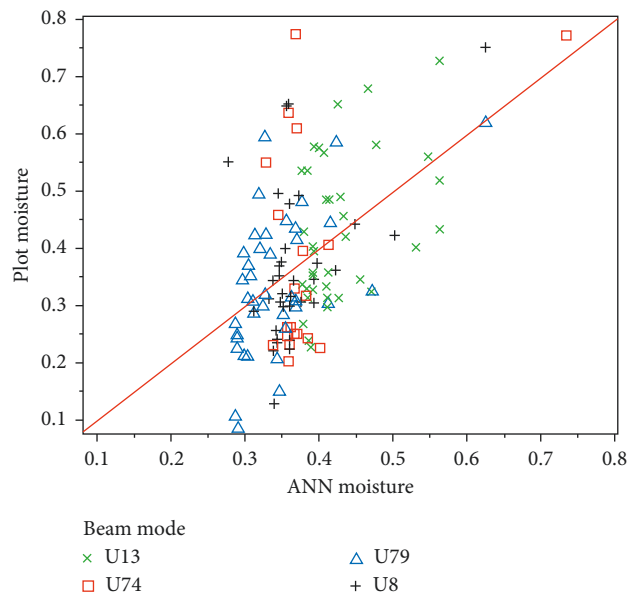

Figure 11: Combined ANN results versus plot-measured soil moisture. July 23 data are not included.

Figure 12: Cape Collingwood outlier plot, showing the heavy moss cover.

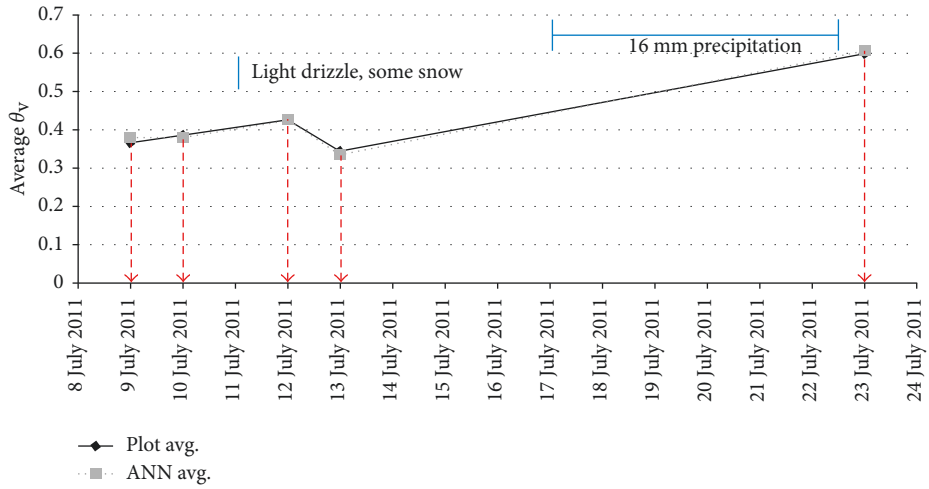

FIGURE 13: Comparison of field-measured average soil moisture to ANN-modelled average soil moisture. Values are within 0.015 θ_v of each other for each date. Arrows indicate RADARSAT-2 data acquisition dates. Timing and duration of precipitation events are also indicated.

space and through time [16]. The Cape Collingwood data again show good agreement with mean values of θ_v (Figure 13), the field-measured and scaled ANN-modelled values being within 0.015 θ_v of each other. The similar mean values indicate that the model is robust with respect to the relative differences between dates and across large numbers of image objects. The ANN results were applied to all image objects in the study area, and the resulting maps clearly indicate stream channels and the wet slopes surrounding them (Figure 14). Aside from the quantitative results already given, this demonstrates in a qualitative sense that the model is working as intended.

3.4. Sources of Error. The relationship between the absolute values of θ_v as determined by the ANN and field measurements is clearly not strong in all cases. With the aforementioned caveats about the relevance of absolute θ_v values in the context of this research in mind, it is still useful to point out some of the underlying causes of the nature of these relationships. The data used as input to the ANN have errors associated with them, specifically with regard to the surface roughness values [72, 73]. We know that even small inaccuracies in roughness parameterization can lead to large errors in soil moisture estimation [81, 82]. In addition to the errors inherent in the surface roughness ANN output [72, 73], there is also the inherent error in the difference between surface-measured roughness and SAR-perceived roughness.

To further the idea of inherent errors in field measurements, there is the problem of integrating soil moisture values across depth. The TDR measurements of θ_v were averaged over the top five cm of the soil surface, and there were often noticeable (qualitatively) moisture gradients between the top of the soil and at 5 cm depth. The SAR backscatter is not necessarily representing the soil to the same depth, a characteristic of the data that depends on θ_v—the lower the soil moisture, the farther the SAR energy penetrates the soil [83], up to a maximum of approximately five cm with RADARSAT-2 (equivalent to the TDR-measured depth). This is a problem that has been known for some time [84], yet is not readily resolved.

Soil moisture changes can also change the form of SAR scattering behaviour. It is known from previous work in the area [27] that saturated or very high soil moisture conditions cause a reduction in the strength of the relationship between SAR backscatter (and other SAR-derived variables) and surface soil moisture. Dobson and Ulaby [85] demonstrated how SAR backscatter reflection changes from diffuse to specular as the soil moisture nears saturation, reducing the backscatter to values associated with lower soil moisture; this is thought to be the reason for the underestimation of high soil moisture values in the ANN model presented here. Under these conditions (i.e., saturated soil moisture), the relationship between the dielectric constant and SAR backscatter is reduced or eliminated; hence, the modelling of soil moisture is confounded within the ANN. This response is also affected by the local incidence angle, with incidence angles closer to nadir being affected less than those at shallower angles. Other studies have revealed that low incidence angles (closer to nadir) are better for soil moisture modelling with SAR data [80], as these angles minimize the backscatter contribution from surface roughness, in addition to minimizing the effects of increased specular reflection due to near-saturated moisture conditions. With the dataset presented in this research, evidence in support of this idea can be seen by analyzing high and low incidence beam modes from the same date (and therefore similar soil moisture conditions). In this case, both a U21 scene (average incidence angle = 45.4°) and an FQ2 scene (average incidence angle = 20.9°) were acquired for the CBAWO on July 23, 2010. When the ANN model output for these two scenes are compared (Figure 15), it is clear that the smaller incidence angle FQ2 scene is modelling higher soil moisture values ($\theta_v > 0.60$) more accurately than the large incidence angle U21 data. Out of 20 field-measured values where $\theta_v > 0.60$, only four of those values are modelled above the 0.60 level for the U21 data, compared to 12 above that level for

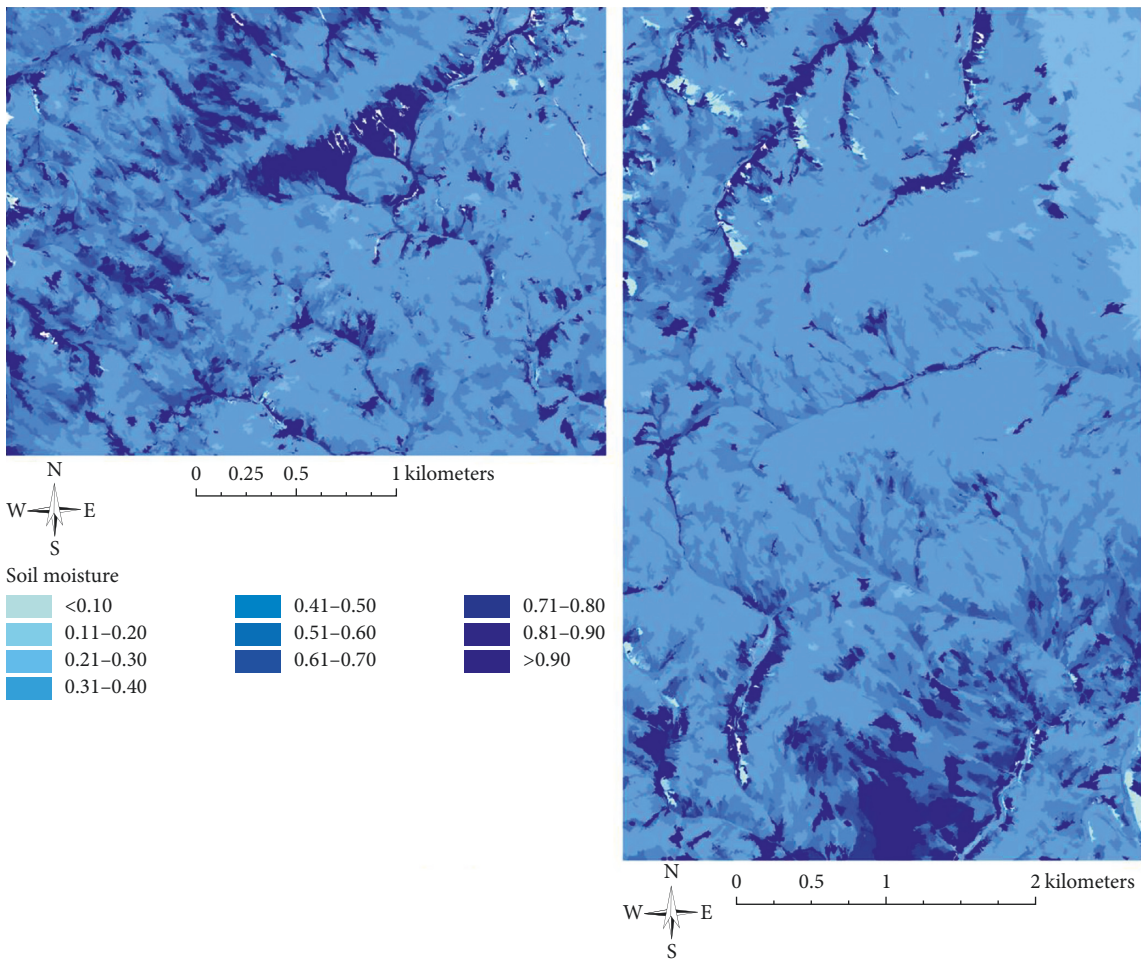

Figure 14: ANN-modelled soil moisture (θ_v) values for the Cape Collingwood study area. The North subset is on the left, and the South subset is on the right. Values are from July 1, 2011.

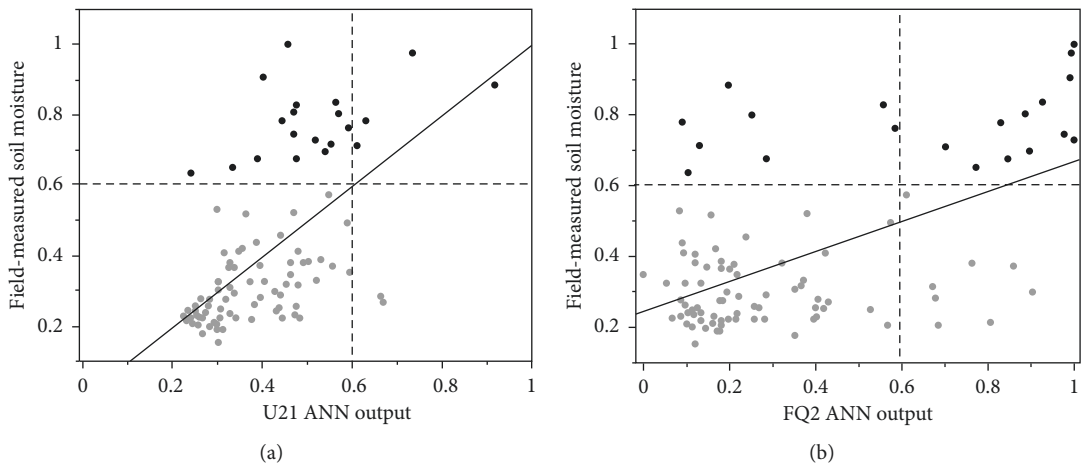

Figure 15: Comparison of incidence angle effects when modelling high soil moisture ($\theta_v > 0.60$) values at the Cape Bounty Arctic Watershed Observatory, July 23, 2010. Here, the U21 and FQ2 scenes have average incidence angles of 45.4° and 20.9°, respectively. Field-measured soil moisture values where volumetric water content was greater than 0.60 (i.e., $\theta_v > 0.60$) are represented in black, whereas values less than 0.60 (i.e., $\theta_v < 0.60$) are presented in grey. Dashed lines indicate where $\theta_v = 0.60$ for both field-measured and ANN-modelled soil moisture values.

the FQ2 data. The overall r^2 is lower for the FQ2 data, however, which could be a result of the comparatively larger spatial resolution or the fact that it is a descending pass (the model was created using ascending pass data). As a result, it is unclear as to why smaller incidence angles do not appear to perform as well when modelling low soil moisture conditions.

4. Conclusions

The soil moisture ANN was implemented using both SAR data (HH-polarized backscatter and local incidence angle) and previously modelled surface roughness values [72, 73]. The model was created from a single date and beam mode (July 11, 2010, U75) and then applied to multiple dates and beam modes, a methodology necessary to model soil moisture through time. The model was applied to the CBAWO, where it was calibrated, and the Cape Collingwood study area, where it was validated under different biophysical and geological conditions.

The 0.155 RMSE average that resulted from the application of the ANN to the different dates at the CBAWO, with the very large soil moisture range present in these environments ($\theta_v = 0$ to 1), is equivalent to other studies at southern latitudes with a θ_v RMSE of 0.05 (a commonly cited value), but maximum soil moisture values of $\theta_v = 0.40$. The absolute moisture values (Figure 8) are not as important as the spatiotemporal distribution of the soil moisture however (i.e., relative differences) (Figure 9), and the strong results of this metric indicate that the model tends to be robust with different input beam modes and across different physical spaces. Similar results were found at the validation site (i.e., Cape Collingwood), with an average r^2 of 0.26 and RMSE of 0.122, though again the spatiotemporal modelling of the moisture was much better (Figure 13).

The best results appear to occur when the model is applied using smaller incidence angle beam modes, which reduce the effects of surface roughness and specular scattering from areas of very high soil moisture. There are, however, very strong relationships between the slope ($r^2 = 0.88$) and intercept ($r^2 = 0.93$) of the regression used to match the ANN output for the different beam modes to the scale of soil moisture measured on the ground. Using these relationships, it is possible to use any beam mode (and associated incidence angle) with the model, as the output can be converted to the proper scale using the slope and intercept equations. However, it is acknowledged that smaller incidence angles may not be as suited to modelling low soil moisture, although the factors for this remain unclear.

When the model is applied to larger image objects, the results are very similar to the smaller image objects, giving rise to the potential to apply the ANN across larger areas (i.e., up-scaling the model output). This adaptability, along with the strong spatiotemporal modelling results, suggests that the ANN model presented in this research is capable of providing useful information for hydrological and climatic model assimilation, in addition to being used as input in other models (hazard susceptibility, vegetation, etc.) and for mapping soil moisture distribution at a high spatial resolution across watersheds.

Conflicts of Interest

The authors declare no conflicts of interest with respect to the publication of this paper.

Acknowledgments

This study received RADARSAT-2 data through the Science and Operational Applications Research–Education initiative (SOAR-E) program of the Canadian Space Agency and the Canada Centre for Remote Sensing. Funding was provided by a variety of sources, including NSERC Alexander Graham Bell Canada Graduate Scholarship (CGS D) (Collingwood), NSERC Discovery Grant (Grant no. RGPIN/03822, Treitz), NSERC Strategic Grant (Grant no. STPGP/380977, Lafrenière), Government of Canada Program for International Polar Year (Grant no. 2006-CC053; Lamoureux), NCE-ArcticNet (Grant no. NCE/12000; Lafrenière and Lamoureux), the Northern Scientific Training Program (NSTP), and the Polar Continental Shelf Project (PCSP). RADARSAT-2 Data and Product© MacDonald, Dettwiler and Associates Ltd. (2013)—All Rights Reserved.

References

[1] M. S. Torn and F. S. Chapin, "Environmental and biotic controls over methane flux from arctic tundra," *Chemosphere*, vol. 26, no. 1–4, pp. 357–368, 1993.

[2] L. Illeris, A. Michelsen, and S. Jonasson, "Soil plus root respiration and microbial biomass following water, nitrogen, and phosphorus application at a high arctic semi desert," *Biogeochemistry*, vol. 65, no. 1, pp. 15–29, 2003.

[3] J. M. Welker, J. T. Fahnestock, G. H. R. Henry, K. W. O'Dea, and R. A. Chimner, "CO_2 exchange in three Canadian High Arctic ecosystems: response to long-term experimental warming," *Global Change Biology*, vol. 10, no. 12, pp. 1981–1995, 2004.

[4] S. Sjögersten, R. van der Wal, and S. J. Woodin, "Small-scale hydrological variation determines landscape CO_2 fluxes in the high Arctic," *Biogeochemistry*, vol. 80, no. 3, pp. 205–216, 2006.

[5] S. F. Oberbauer, C. E. Tweedie, J. M. Welker et al., "Tundra CO_2 fluxes in response to experimental warming across latitudinal and moisture gradients," *Ecological Monographs*, vol. 77, no. 2, pp. 221–238, 2007.

[6] J. Dagg and P. Lafleur, "Vegetation community, foliar nitrogen, and temperature effects on tundra CO_2 exchange across a soil moisture gradient," *Arctic, Antarctic, and Alpine Research*, vol. 43, no. 2, pp. 189–197, 2011.

[7] M. Reichstein, M. Bahn, P. Ciais et al., "Climate extremes and the carbon cycle," *Nature*, vol. 500, no. 7462, pp. 287–295, 2013.

[8] R. G. Taylor, B. Scanlon, P. Döll et al., "Ground water and climate change," *Nature Climate Change*, vol. 3, no. 4, pp. 322–329, 2013.

[9] M.-K. Woo and Z. Xia, "Suprapermafrost groundwater seepage in gravelly terrain, Resolute, NWT, Canada," *Permafrost and Periglacial Processes*, vol. 6, no. 1, pp. 57–72, 1995.

[10] M. Woo and Z. Xia, "Effects of hydrology on the thermal conditions of the active layer," *Hydrology Research*, vol. 27, no. 1–2, pp. 129–142, 1996.

[11] K. M. Hinkel, F. Paetzold, F. E. Nelson, and J. G. Bockheim, "Patterns of soil temperature and moisture in the active layer and upper permafrost at Barrow, Alaska: 1993–1999," *Global and Planetary Change*, vol. 29, no. 3, pp. 293–309, 2001.

[12] S. M. Natali, E. A. G. Schuur, and R. L. Rubin, "Increased plant productivity in Alaskan tundra as a result of experimental warming of soil and permafrost," *Journal of Ecology*, vol. 100, no. 2, pp. 488–498, 2012.

[13] K. E. O. Todd-Brown, J. T. Randerson, F. Hopkins et al., "Changes in soil organic carbon storage predicted by Earth system models during the 21st century," *Biogeosciences*, vol. 11, no. 8, pp. 2341–2356, 2014.

[14] R. P. Daanen, D. Misra, and H. Epstein, "Active-layer hydrology in nonsorted circle ecosystems of the arctic tundra," *Vadose Zone Journal*, vol. 6, no. 4, pp. 694–704, 2007.

[15] P. Dobriyal, A. Qureshi, R. Badola, and S. A. Hussain, "A review of the methods available for estimating soil moisture and its implications for water resource management," *Journal of Hydrology*, vol. 458, pp. 110–117, 2012.

[16] K. C. Kornelsen and P. Coulibaly, "Advances in soil moisture retrieval from synthetic aperture radar and hydrological applications," *Journal of Hydrology*, vol. 476, pp. 460–489, 2013.

[17] S. S. Haider, S. Said, U. C. Kothyari, and M. K. Arora, "Soil moisture estimation using ERS 2 SAR data: a case study in the Solani River catchment/estimation de l'humidité du sol grâce à des données ERS-2 SAR: étude de cas dans le bassin de la rivière Solani," *Hydrological Sciences Journal*, vol. 49, no. 2, 2004.

[18] S. Said, U. C. Kothyari, and M. K. Arora, "ANN-based soil moisture retrieval over bare and vegetated areas using ERS-2 SAR data," *Journal of Hydrologic Engineering*, vol. 13, no. 6, pp. 461–475, 2008.

[19] L. Brocca, T. Tullo, F. Melone, T. Moramarco, and R. Morbidelli, "Catchment scale soil moisture spatial–temporal variability," *Journal of Hydrology*, vol. 422-423, pp. 63–75, 2012.

[20] P. C. Dubois, J. Van Zyl, and T. Engman, "Measuring soil moisture with imaging radars," *IEEE Transactions on Geoscience and Remote Sensing*, vol. 33, no. 4, pp. 915–926, 1995.

[21] D. Entekhabi, E. G. Njoku, P. E. O'Neill et al., "The soil moisture active passive (SMAP) mission," *Proceedings of the IEEE*, vol. 98, no. 5, pp. 704–716, 2010.

[22] F. De Zan, A. Parizzi, P. Prats-Iraola, and P. López-Dekker, "A SAR interferometric model for soil moisture," *IEEE Transactions on Geoscience and Remote Sensing*, vol. 52, no. 1, pp. 418–425, 2014.

[23] B. W. Barrett, E. Dwyer, and P. Whelan, "Soil moisture retrieval from active spaceborne microwave observations: an evaluation of current techniques," *Remote Sensing*, vol. 1, no. 3, pp. 210–242, 2009.

[24] A. Moreira, G. Krieger, I. Hajnsek et al., "Tandem-L: a highly innovative bistatic SAR mission for global observation of dynamic processes on the Earth's surface," *IEEE Geoscience and Remote Sensing Magazine*, vol. 3, no. 2, pp. 8–23, 2015.

[25] D. L. Kane, L. D. Hinzman, H. Yu, and D. J. Goering, "The use of SAR satellite imagery to measure active layer moisture contents in Arctic Alaska," *Hydrology Research*, vol. 27, no. 1-2, pp. 25–38, 1996.

[26] N. G. Meade, L. D. Hinzman, and D. L. Kane, "Spatial estimation of soil moisture using synthetic aperture radar in Alaska," *Advances in Space Research*, vol. 24, no. 7, pp. 935–940, 1999.

[27] J. Wall, A. Collingwood, and P. Treitz, "Monitoring surface moisture state in the Canadian high Arctic using synthetic aperture radar (SAR)," *Canadian Journal of Remote Sensing*, vol. 36, no. 1, pp. S124–S134, 2010.

[28] E. Högström and A. Bartsch, "Impact of backscatter variations over water bodies on coarse-scale radar retrieved soil moisture and the potential of correcting with meteorological data," *IEEE Transactions on Geoscience and Remote Sensing*, vol. 55, no. 1, pp. 3–13, 2017.

[29] T. Jagdhuber, J. Stockamp, I. Hajnsek, and R. Ludwig, "Identification of soil freezing and thawing states using SAR polarimetry at C-Band," *Remote Sensing*, vol. 6, no. 3, pp. 2008–2023, 2014.

[30] E. E. Sano, A. R. Huete, D. Troufleau, M. S. Moran, and A. Vidal, "Relation between ERS-1 synthetic aperture radar data and measurements of surface roughness and moisture content of rocky soils in a semiarid rangeland," *Water Resources Research*, vol. 34, no. 6, pp. 1491–1498, 1998.

[31] M. Shoshany, T. Svoray, P. J. Curran, G. M. Foody, and A. Perevolotsky, "The relationship between ERS-2 SAR backscatter and soil moisture: generalization from a humid to semi-arid transect," *International Journal of Remote Sensing*, vol. 21, no. 11, pp. 2337–2343, 2000.

[32] H. Lievens, N. E. C. Verhoest, E. De Keyser et al., "Effective roughness modelling as a tool for soil moisture retrieval from C-and L-band SAR," *Hydrology and Earth System Sciences*, vol. 15, no. 1, pp. 151–162, 2011.

[33] K. Millard and M. Richardson, "Quantifying the relative contributions of vegetation and soil moisture conditions to polarimetric C-Band SAR response in a temperate peatland," *Remote Sensing of Environment*, vol. 206, pp. 123–138, 2018.

[34] D. P. Thoma, M. S. Moran, R. Bryant et al., "Comparison of four models to determine surface soil moisture from C-band radar imagery in a sparsely vegetated semiarid landscape," *Water Resources Research*, vol. 42, no. 1, 2006.

[35] A. K. Fung, Z. Li, and K.-S. Chen, "Backscattering from a randomly rough dielectric surface," *IEEE Transactions on Geoscience and Remote Sensing*, vol. 30, no. 2, pp. 356–369, 1992.

[36] N. Baghdadi, S. Gaultier, and C. King, "Retrieving surface roughness and soil moisture from synthetic aperture radar (SAR) data using neural networks," *Canadian Journal of Remote Sensing*, vol. 28, no. 5, pp. 701–711, 2002.

[37] Z. Li, X. Ren, X. Li, and L. Wang, "Soil moisture mapping with C band multi-polarization SAR imagery," *Polarization*, vol. 900, no. 2, p. 35, 2005.

[38] M. B. Charlton and K. White, "Sensitivity of radar backscatter to desert surface roughness," *International Journal of Remote Sensing*, vol. 27, no. 8, pp. 1641–1659, 2006.

[39] S.-B. Kim, M. Moghaddam, L. Tsang, M. Burgin, X. Xu, and E. G. Njoku, "Models of L-band radar backscattering coefficients over global terrain for soil moisture retrieval," *IEEE Transactions on Geoscience and Remote Sensing*, vol. 52, no. 2, pp. 1381–1396, 2014.

[40] S.-B. Kim, J. J. van Zyl, J. T. Johnson et al., "Surface soil moisture retrieval using the l-band synthetic aperture radar onboard the soil moisture active–passive satellite and evaluation at core validation sites," *IEEE Transactions on Geoscience and Remote Sensing*, vol. 55, no. 4, pp. 1897–1914, 2017.

[41] M. R. Sahebi, F. Bonn, and G. B. Bénié, "Neural networks for the inversion of soil surface parameters from synthetic aperture radar satellite data," *Canadian Journal of Civil Engineering*, vol. 31, no. 1, pp. 95–108, 2004.

[42] S. Gopal and C. Woodcock, "Remote sensing of forest change using artificial neural networks," *IEEE Transactions on Geoscience and Remote Sensing*, vol. 34, no. 2, pp. 398–404, 1996.

[43] B. Pradhan and S. Lee, "Landslide susceptibility assessment and factor effect analysis: backpropagation artificial neural networks and their comparison with frequency ratio and bivariate logistic regression modelling," *Environmental Modelling and Software*, vol. 25, no. 6, pp. 747–759, 2010.

[44] F. Del Frate and L.-F. Wang, "Sunflower biomass estimation using a scattering model and a neural network algorithm," *International Journal of Remote Sensing*, vol. 22, no. 7, pp. 1235–1244, 2001.

[45] J. F. Mas and J. J. Flores, "The application of artificial neural networks to the analysis of remotely sensed data," *International Journal of Remote Sensing*, vol. 29, no. 3, pp. 617–663, 2008.

[46] S. Paloscia, P. Pampaloni, S. Pettinato, and E. Santi, "A comparison of algorithms for retrieving soil moisture from ENVISAT/ASAR images," *IEEE Transactions on Geoscience and Remote Sensing*, vol. 46, no. 10, pp. 3274–3284, 2008.

[47] D. A. Hodgson and J.-S. Vincent, "A 10,000 yr B.P. extensive ice shelf over Viscount Melville Sound, Arctic Canada," *Quaternary Research*, vol. 22, no. 1, pp. 18–30, 1984.

[48] P. Lajeunesse and M. A. Hanson, "Field observations of recent transgression on northern and eastern Melville Island, western Canadian Arctic Archipelago," *Geomorphology*, vol. 101, no. 4, pp. 618–630, 2008.

[49] D. M. Barnett, S. A. Edlund, L. A. Dredge, D. C. Thomas, and L. S. Prevett, *Terrain Classification and Evaluation, Eastern Melville Island, NWT*, Geological Survey of Canada Open File 252, p. 1318, 1975.

[50] G. C. Heathman, P. J. Starks, and M. A. Brown, "Time domain reflectometry field calibration in the Little Washita River Experimental Watershed," *Soil Science Society of America Journal*, vol. 67, no. 1, pp. 52–61, 2003.

[51] G. C. Topp, J. L. Davis, and A. P. Annan, "Electromagnetic determination of soil water content: measurements in coaxial transmission lines," *Water Resources Research*, vol. 16, no. 3, pp. 574–582, 1980.

[52] C. Yu, A. W. Warrick, and M. H. Conklin, "Derived functions of time domain reflectometry for soil moisture measurement," *Water Resources Research*, vol. 35, no. 6, pp. 1789–1796, 1999.

[53] R. M. Nagare, R. A. Schincariol, W. L. Quinton, and M. Hayashi, "Laboratory calibration of time domain reflectometry to determine moisture content in undisturbed peat samples," *European Journal of Soil Science*, vol. 62, no. 4, pp. 505–515, 2011.

[54] J. Stein and D. L. Kane, "Monitoring the unfrozen water content of soil and snow using time domain reflectometry," *Water Resources Research*, vol. 19, no. 6, pp. 1573–1584, 1983.

[55] M. A. Malicki, R. Plagge, and C. H. Roth, "Improving the calibration of dielectric TDR soil moisture determination taking into account the solid soil," *European Journal of Soil Science*, vol. 47, no. 3, pp. 357–366, 1996.

[56] F. Del Frate and D. Solimini, "On neural network algorithms for retrieving forest biomass from SAR data," *IEEE Transactions on Geoscience and Remote Sensing*, vol. 42, no. 1, pp. 24–34, 2004.

[57] R. Leconte, F. Brissette, M. Galarneau, and J. Rousselle, "Mapping near-surface soil moisture with RADARSAT-1 synthetic aperture radar data," *Water Resources Research*, vol. 40, no. 1, 2004.

[58] Y. Oh, "Quantitative retrieval of soil moisture content and surface roughness from multipolarized radar observations of bare soil surfaces," *IEEE Transactions on Geoscience and Remote Sensing*, vol. 42, no. 3, pp. 596–601, 2004.

[59] Y. Oh, K. Sarabandi, and F. T. Ulaby, "An empirical model and an inversion technique for radar scattering from bare soil surfaces," *IEEE Transactions on Geoscience and Remote Sensing*, vol. 30, no. 2, pp. 370–381, 1992.

[60] M. R. Sahebi and J. Angles, "An inversion method based on multi-angular approaches for estimating bare soil surface parameters from RADARSAT-1," *Hydrology and Earth System Sciences*, vol. 14, no. 11, pp. 2355–2366, 2010.

[61] G. J. Bowden, G. C. Dandy, and H. R. Maier, "Input determination for neural network models in water resources applications. Part 1—background and methodology," *Journal of Hydrology*, vol. 301, no. 1–4, pp. 75–92, 2005.

[62] G. Mountrakis, J. Im, and C. Ogole, "Support vector machines in remote sensing: a review," *ISPRS Journal of Photogrammetry and Remote Sensing*, vol. 66, no. 3, pp. 247–259, 2011.

[63] X. Zhuang, B. A. Engel, D. F. Lozano-Garcia, R. N. Fernandez, and C. J. Johannsen, "Optimization of training data required for neuro-classification," *Remote Sensing*, vol. 15, no. 16, pp. 3271–3277, 1994.

[64] D. R. Hush, "Classification with neural networks: a performance analysis," in *Proceedings of the IEEE International Conference on Systems Engineering*, pp. 277–280, Wrocław, Poland, 1989.

[65] M. T. Hagan and M. B. Menhaj, "Training feedforward networks with the Marquardt algorithm," *IEEE Transactions on Neural Networks*, vol. 5, no. 6, pp. 989–993, 1994.

[66] T. Blaschke, "Object based image analysis for remote sensing," *ISPRS Journal of Photogrammetry and Remote Sensing*, vol. 65, no. 1, pp. 2–16, 2010.

[67] L. Drăguţ, D. Tiede, and S. R. Levick, "ESP: a tool to estimate scale parameter for multiresolution image segmentation of remotely sensed data," *International Journal of Geographical Information Science*, vol. 24, no. 6, pp. 859–871, 2010.

[68] E. Cognition, *eCognition Developer (8.64. 0) User Guide*, Trimble Germany GmbH, München, Germany, 2010.

[69] L. Drăgut, T. Schauppenlehner, A. Muhar, J. Strobl, and T. Blaschke, "Optimization of scale and parametrization for terrain segmentation: an application to soil-landscape modeling," *Computers and Geosciences*, vol. 35, no. 9, pp. 1875–1883, 2009.

[70] J. Álvarez-Mozos, A. Larrañaga, M. González-Audicana, and J. Casali, "On the influence of surface roughness on RADARSAT-2 polarimetric observations," in *Proceedings of the 4th International Workshop on Science and Applications of SAR Polarimetry and Polarimetric Interferometry*, pp. 26–30, Frascati, Italy, January 2009.

[71] N. E. C. Verhoest, H. Lievens, W. Wagner, J. Álvarez-Mozos, M. S. Moran, and F. Mattia, "On the soil roughness parameterization problem in soil moisture retrieval of bare surfaces from synthetic aperture radar," *Sensors*, vol. 8, no. 7, pp. 4213–4248, 2008.

[72] A. Collingwood, P. Treitz, and F. Charbonneau, "Surface roughness estimation from RADARSAT-2 data in a high Arctic environment," *International Journal of Applied Earth Observation and Geoinformation*, vol. 27, pp. 70–80, 2014.

[73] A. W. Collingwood, *Modeling Biophysical Variables in the Canadian High Arctic using Synthetic Aperture Radar Data*, Queen's University, Kingston, ON, Canada, 2014.

[74] T. Lakhankar, H. Ghedira, M. Temimi, M. Sengupta, R. Khanbilvardi, and R. Blake, "Non-parametric methods for soil moisture retrieval from satellite remote sensing data," *Remote Sensing*, vol. 1, no. 1, pp. 3–21, 2009.

[75] R. M. Haralick, K. Shanmugam, and I. Dinstein, "Textural features for image classification," *IEEE Transactions on Systems, Man, and Cybernetics*, vol. 3, no. 6, pp. 610–621, 1973.

[76] C. Oliver and S. Quegan, *Understanding Synthetic Aperture Radar Images*, Artech House, Boston, MA, USA, 1998.
[77] Y. Wang, F. Wang, J. Huang, X. Wang, and Z. Liu, "Validation of artificial neural network techniques in the estimation of nitrogen concentration in rape using canopy hyperspectral reflectance data," *International Journal of Remote Sensing*, vol. 30, no. 17, pp. 4493–4505, 2009.
[78] S. R. Cloude and E. Pottier, "An entropy based classification scheme for land applications of polarimetric SAR," *IEEE Transactions on Geoscience and Remote Sensing*, vol. 35, no. 1, pp. 68–78, 1997.
[79] J. R. Adams, A. A. Berg, H. McNairn, and A. Merzouki, "Sensitivity of C-band SAR polarimetric variables to unvegetated agricultural fields," *Canadian Journal of Remote Sensing*, vol. 39, no. 1, pp. 1–16, 2013.
[80] F. T. Ulaby and P. P. Batlivala, "Optimum radar parameters for mapping soil moisture," *IEEE Transactions on Geoscience Electronics*, vol. 14, no. 2, pp. 81–93, 1976.
[81] K. J. Tansey and A. C. Millington, "Investigating the potential for soil moisture and surface roughness monitoring in drylands using ERS SAR data," *International Journal of Remote Sensing*, vol. 22, no. 11, pp. 2129–2149, 2001.
[82] J. Alvarez-Mozos, J. Casali, M. González-Audicana, and N. E. C. Verhoest, "Assessment of the operational applicability of RADARSAT-1 data for surface soil moisture estimation," *IEEE Transactions on Geoscience and Remote Sensing*, vol. 44, no. 4, pp. 913–924, 2006.
[83] F. T. Ulaby, P. C. Dubois, and J. Van Zyl, "Radar mapping of surface soil moisture," *Journal of Hydrology*, vol. 184, no. 1-2, pp. 57–84, 1996.
[84] F. T. Ulaby, P. P. Batlivala, and M. C. Dobson, "Microwave backscatter dependence on surface roughness, soil moisture, and soil texture: part I-bare soil," *IEEE Transactions on Geoscience Electronics*, vol. 16, no. 4, pp. 286–295, 1978.
[85] M. C. Dobson and F. Ulaby, "Microwave backscatter dependence on surface roughness, soil moisture, and soil texture: part III-soil tension," *IEEE Transactions on Geoscience and Remote Sensing*, vol. GE-19, no. 1, pp. 51–61, 1981.